IOPscience iopscience.iop.org

Home Search Collections Journals About Contact us My IOPscience

Persistent currents in a graphene ring with armchair edges

This article has been downloaded from IOPscience. Please scroll down to see the full text article.

2012 J. Phys.: Condens. Matter 24 245304

(http://iopscience.iop.org/0953-8984/24/24/245304)

View the table of contents for this issue, or go to the journal homepage for more

Download details:
IP Address: 140.122.141.75
The article was downloaded on 24/05/2012 at 03:35

Please note that terms and conditions apply.

IOP PUBLISHING JOURNAL OF PHYSICS: CONDENSED MATTER

J. Phys.: Condens. Matter **24** (2012) 245304 (8pp) doi:10.1088/0953-8984/24/24/245304

Persistent currents in a graphene ring with armchair edges

Bor-Luen Huang[1], **Ming-Che Chang**[1] **and Chung-Yu Mou**[2,3,4]

[1] Department of Physics, National Taiwan Normal University, Taipei 11677, Taiwan
[2] Department of Physics, National Tsing Hua University, Hsinchu 30013, Taiwan
[3] Institute of Physics, Academia Sinica, Nankang 11529, Taiwan
[4] Physics Division, National Center for Theoretical Sciences, PO Box 2-131, Hsinchu 30013, Taiwan

E-mail: borluen.huang@gmail.com, changmc@phy.ntnu.edu.tw and mou@phys.nthu.edu.tw

Received 16 January 2012, in final form 16 April 2012
Published 23 May 2012
Online at stacks.iop.org/JPhysCM/24/245304

Abstract
A graphene nanoribbon with armchair edges is known to have no edge state. However, if the nanoribbon is in the quantum spin Hall state, then there must be helical edge states. By folding a graphene ribbon into a ring and threading it by a magnetic flux, we study the persistent charge and spin currents in the tight-binding limit. It is found that, for a broad ribbon, the edge spin current approaches a finite value independent of the radius of the ring. For a narrow ribbon, inter-edge coupling between the edge states could open the Dirac gap and reduce the overall persistent currents. Furthermore, by enhancing the Rashba coupling, we find that the persistent spin current gradually reduces to zero at a critical value beyond which the graphene is no longer a quantum spin Hall insulator.

(Some figures may appear in colour only in the online journal)

1. Introduction

A crucial feature of a topological insulator is the existence of metallic surface states [1]. These surface states (or *edge states* if the insulator is two-dimensional) have odd pairs of channels, in which each pair consists of opposite spins moving in opposite directions (helical edge states). Therefore, they could carry charge as well as spin currents. We are interested in studying their transport using a lattice model. In theory, one could rely on a model with external leads and reservoirs, or with a closed ring in which the currents are driven by a threading magnetic flux. In this work, we adopt the latter (simpler) approach and use the graphene lattice as a theoretical model to study the transport of these important helical edge states.

Graphene is one of the earliest candidates for a two-dimensional topological insulator (also called a quantum spin Hall insulator) [2]. It is found that graphene would become a quantum spin Hall (QSH) insulator if there is a spin–orbit interaction (SOI). However, since graphene's SOI is only of the order of 10^{-3} meV [3], it poses an experimental challenge to probe such a state[5]. Experimental issues aside, a graphene lattice is ideal for theoretical investigation of the helical edge states. To avoid complications from pre-existing edge states, we choose a graphene ribbon with armchair edges, which has no edge state in the absence of SOI. That is, the edge states studied here are intrinsic to the QSH insulator. In contrast, a graphene ribbon with zigzag edges has edge states even without SOI [5]. These edge states would become helical edge states (similar to those in this work) with SOI.

If the graphene ribbon is wrapped up to form a tube (or a ring, with armchair edges), with a magnetic flux passing through the hole, then the helical edge state provides a robust channel for persistent charge current (PCC) and persistent spin current (PSC). PCC in a mesoscopic metal ring was first predicted [6] and later verified in experiments [7] decades ago. In a recent work [8], the PCC was measured accurately by mounting nanorings on a micro-cantilever in an external magnetic field. In addition to the PCC, the PSC in a ring in a textured magnetic field [9] or in a ring with SOI [10] has been proposed. Further researchers show that it is possible to have a

[5] Recently, it has been proposed that, with the help of adatoms, the QSH phase of graphene could be enhanced [4].

 © 2012 IOP Publishing Ltd Printed in the UK & the USA

PSC in a ferromagnetic ring [11] or an antiferromagnetic ring [12].

There have been several studies of the Aharonov–Bohm effect and PCC in a graphene ring with different geometrical shapes (without spin–orbit interaction). For example, a nanotorus [13], flat rings (similar to Corbino discs) with various types of boundaries [14–16] or a tube with zigzag edges [17]. Observation of the Aharonov–Bohm effect is indirect evidence of the PCC. Recently, the Aharonov–Bohm oscillation in a nanorod of a topological insulator has been observed [18] and studied [19, 20]. Theoretical investigations of the persistent currents in a two-dimensional topological insulator ring, which are based on an effective continuous model, can be found in [21, 22]. In [23], the zigzag edge of a graphene sheet is found to be magnetized due to the Hubbard interaction. Since the time-reversal symmetry is spontaneously broken, edge charge current appears without the need for a driving magnetic flux.

In this paper, we study the quantum spin Hall states and the persistent currents of an armchair ring with SOI. Different from earlier approaches [21, 22], this work is based on a lattice model, which allows insulating band structure and genuine edge states. By changing its parameters, the graphene ring can be in or out of the QSH phase, and the behavior of the persistent currents across the phase boundary can be studied. It is found that, for a broad ribbon, the edge PCC is small (but nonzero), while the edge PSC approaches a finite value. For a narrow ribbon, the edge states from opposite sides couple with each other, which may open an energy gap and reduce the persistent currents. We have also considered the Zeeman coupling and the Rashba coupling. The former introduces additional jumps in the periodic sawtooth curves of the persistent currents. By breaking spin conservation, the Rashba coupling reduces the edge spin current, which eventually vanishes at the boundary of the QSH phase. Many of the results obtained here should also apply qualitatively to the helical edge states and persistent currents of a three-dimensional topological insulator ring.

This paper is outlined as follows. In section 2, we describe the theoretical model being used. In section 3 we first study the helical edge states and related PCC and PSC in rings with various sizes, then comment on the effects of the Zeeman and the Rashba interactions. Section 4 is the conclusion.

2. Theoretical formulation

We start with a tight-binding model for a graphene ribbon. One imposes the open boundary condition with armchair edges along the x direction and periodic boundary condition along the y direction (see figure 1). A magnetic flux Φ passes through the inside of the ring along the $(-x)$ direction. Because of the magnetic flux, an electron circling the ribbon once would acquire an Aharonov–Bohm phase of $2\pi\Phi/\Phi_0$, where Φ_0 is the flux quantum. The Hamiltonian is [2]

$$H = -t\sum_{\langle i,j\rangle} \mathrm{e}^{\mathrm{i}\theta_1} c_i^\dagger c_j + \mathrm{i}\lambda_{\mathrm{SO}} \sum_{\langle i,j\rangle} \mathrm{e}^{\mathrm{i}\theta_2} \nu_{ij} c_i^\dagger \sigma^z c_j + \frac{g}{2}\mu_{\mathrm{B}} B \sum_i c_i^\dagger \sigma^x c_i + \mathrm{i}\lambda_{\mathrm{R}} \sum_{\langle i,j\rangle} \mathrm{e}^{\mathrm{i}\theta_1} c_i^\dagger (\boldsymbol{\sigma}\times\hat{\mathbf{d}}_{ij})_z c_j, \quad (1)$$

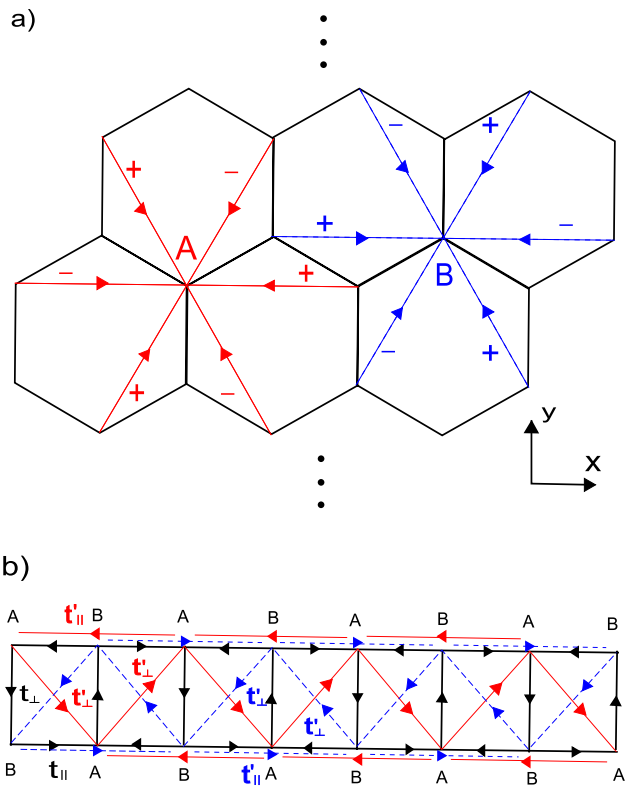

Figure 1. The honeycomb lattice is shown in (a). Red and blue arrows are the next-nearest-neighbor hoppings. The red and blue arrows in the plot are for spin-up electrons in A and B sub-lattices, and + and − signs refer to the signs of ν_{ij}. For spin-down electrons, red and blue arrows appear in opposite directions. The effective two-lag ladder for the Hamiltonian in equation (3) is shown in (b).

where $c_i^\dagger = (c_{i\uparrow}^\dagger, c_{i\downarrow}^\dagger)$ creates an electron at lattice site i. The first term accounts for the nearest-neighbor hoppings. The second term is a SOI with next-nearest-neighbor hoppings, in which $\nu_{ij} = (2/\sqrt{3})(\hat{d}_1 \times \hat{d}_2)\cdot\hat{z}$, $\hat{d}_1$ and $\hat{d}_2$ are the two nearest-neighbor bonds that connect site-j to site-i, and $\boldsymbol{\sigma}$ are the Pauli matrices. The third and the fourth terms are the Zeeman and the Rashba couplings. In the following, all energies and lengths will be in units of t and a (lattice constant), respectively.

The phases θ_1 and θ_2 are related to the magnetic flux: $\theta_1 = 2\phi/3$ for the nearest-neighbor bonds along the y direction (see figure 1), while $\theta_1 = \phi/3$ for the zigzag bonds, where $\phi = (2\pi/N_y)\Phi/\Phi_0$, N_y is the number of unit cells around the ring. The phase θ_2 is zero for the next-nearest-neighbor bonds along the x direction, while $\theta_2 = \phi$ for the other next-nearest-neighbor bonds. These phases are chosen in such a way that the electron would pick up the correct Aharonov–Bohm phase when circling the ring once, no matter which path it takes. The geometric curvature of the tube is known to enhance the SOI [24], but such a curvature effect is not considered.

Because of the translational invariance along the y direction, one can perform the following Fourier transformation:

$$c_{x,y} = \frac{1}{\sqrt{N_y}} \sum_{k_y} \mathrm{e}^{\mathrm{i}k_y y} c_{x,k_y} \quad (2)$$

and map the system to a two-lag ladder[6]. The effective Hamiltonian can be written as

$$H = \sum_{k_y} \Psi^\dagger \begin{pmatrix} T' & T & \mu_B B & R \\ T^\dagger & -T' & R^* & \mu_B B \\ \mu_B B & R^T & -T' & T \\ R^\dagger & \mu_B B & T^\dagger & T' \end{pmatrix} \Psi, \tag{3}$$

where $\Psi^\dagger(x, k_y) = (\psi^\dagger_{A\uparrow}, \psi^\dagger_{B\uparrow}, \psi^\dagger_{A\downarrow}, \psi^\dagger_{B\downarrow})$. The matrix elements are

$$T' = \begin{pmatrix} 0 & t'^*_\perp & t'_\parallel & 0 & \cdots & 0 \\ t'_\perp & 0 & t'^*_\perp & t'_\parallel & \ddots & \vdots \\ t'^*_\parallel & t'_\perp & 0 & t'^*_\perp & \ddots & 0 \\ 0 & t'^*_\parallel & t'_\perp & 0 & \ddots & t'_\parallel \\ \vdots & \ddots & \ddots & \ddots & \ddots & t'^*_\perp \\ 0 & \cdots & 0 & t'^*_\parallel & t'_\perp & 0 \end{pmatrix}, \tag{4}$$

where $t_\parallel = te^{i\frac{1}{3}\phi_k}, t_\perp = te^{i\frac{2}{3}\phi_k}$, $t'_\parallel = i\lambda_{SO}$ and $t'_\perp = 2i\lambda_{SO}\cos\phi_k$, where $\phi_k = \frac{\sqrt{3}}{2}k_y a - \phi/2$ and

$$T = \begin{pmatrix} t^*_\perp & t_\parallel & 0 & \cdots & 0 \\ t_\parallel & t^*_\perp & t_\parallel & \ddots & \vdots \\ 0 & t_\parallel & t^*_\perp & \ddots & 0 \\ \vdots & \ddots & \ddots & \ddots & t_\parallel \\ 0 & \cdots & 0 & t_\parallel & t^*_\perp \end{pmatrix}. \tag{5}$$

In equation (3), $\mu_B B$ is multiplied by an unit matrix. The Rashba term gives

$$R = \begin{pmatrix} R^*_\perp & R_- & 0 & \cdots & 0 \\ R_+ & R^*_\perp & R_- & \ddots & \vdots \\ 0 & R_+ & R^*_\perp & \ddots & 0 \\ \vdots & \ddots & \ddots & \ddots & R_- \\ 0 & \cdots & 0 & R_+ & R^*_\perp \end{pmatrix}, \tag{6}$$

where $R_\perp = -\frac{i}{\sqrt{3}}\lambda_R e^{2i\phi_k/3}$, $R_\pm = R_y \pm iR_x$, $R_x = \frac{i}{2}\lambda_R e^{i\phi_k/3}$ and $R_y = -\frac{i}{2\sqrt{3}}\lambda_R e^{i\phi_k/3}$.

At zero temperature, the PCC of the nanoring is given by (in units of et/h)

$$I = -\sum_{mk_y} \frac{\partial E_{mk_y}}{\partial \Phi}, \tag{7}$$

in which one sums over filled states (for total current) or edge states (for edge current). The PSC for spin-z will be calculated by the following semiclassical expression [10] (in units of $(\hbar/2)t/h = t/4\pi$):

$$I^s = -\sum_{mk_y} \frac{\partial E_{mk_y}}{\partial \Phi} \langle mk_y|\sigma_z|mk_y\rangle, \tag{8}$$

where $|mk_y\rangle$ are the Bloch states.

When the spin is conserved (sections 3.1 and 3.2), the following notations are used: the current for spin-up and spin-down electrons is I_σ. Therefore, the total charge current is $I = I_+ + I_-$ and the total spin current is $I^s = I_+ - I_-$. The spin-dependent edge currents are $I_{R\sigma}$ and $I_{L\sigma}$. For example, the charge and spin currents for the right edge are $I_R = I_{R+} + I_{R-}$ and $I^s_R = I_{R+} - I_{R-}$, respectively.

In general, I_σ is the sum of edge current and bulk current. The existence of persistent *bulk* current in an insulator ring (the usual type or the QSH type) is due to the discreteness (due to the finite circumference) and asymmetry (due to the magnetic flux) of the energy spectrum. As a result, it only exists in a ring with finite radius (with or without SOI), and diminishes when the ring is larger. In contrast, there is no spin-resolved current (either bulk or edge) in a usual insulator ring. It only exists in the QSH phase and is not reduced in a larger ring. That is, the persistent spin current reported below is intrinsic to the QSH phase.

3. Numerical results

There are several tunable parameters in the numerical calculations: width and length (circumference) of the ribbon, spin–orbit couplings λ_{SO} and λ_R, and the g factor (for the Zeeman coupling). In addition, the magnetic flux inside the ring controls the magnitude of the persistent currents. To explore such a large parameter space, the following path is adopted: we first show the energy spectrum and the decay length of the edge states, then present the charge and spin transport for broad ribbons (section 3.1). Subsequently, the transport in narrow ribbons is shown and the finite-size effect discussed (section 3.2). In either case, to simplify the discussion, Zeeman and Rashba couplings are not included. Their effect will be investigated in sections 3.3 and 3.4, respectively. Among these parameters, the most important ones are λ_{SO} and λ_R, which dictate whether the graphene is in the QSH phase [2]. Their overall influence on edge states and spin current can be seen in figures 3 and 10.

Before showing the result, we review the energy spectrum of a *flat* graphene nanoribbon with armchair edges, but without SOI [5]. First, the width of the ribbon has a major effect on the energy gap. If $n_x = 3n + 2$, then there is a Dirac point at $k_y = 0$ and the system is gapless in the tight-binding model. If $n_x \neq 3n + 2$, then the system has a finite gap, which approaches zero as n_x becomes infinite. Second, in the presence of SOI, the Dirac point of a ribbon with $n_x = 3n+2$ is opened and mid-gap edge states are crossing at $k_y = 0$. Similar mid-gap edge states exist for $n_x \neq 3n + 2$.

3.1. Broad ribbon

In Kane and Mele's analysis [2], the graphene enters the QSH state once the SOI is turned on, without a finite threshold

[6] This is an extension of the one-chain effective model in figure 12 of [25].

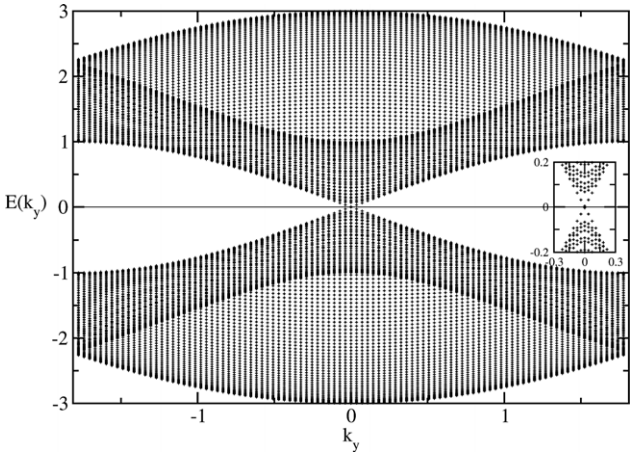

Figure 2. Energy spectrum for a graphene ribbon with $n_x = 100$, $n_y = 100$ and $\lambda_{SO} = 0.01$. The inset shows the magnified view near the Dirac point. The bulk gap is about 0.136, which is slightly larger than the bulk value of $6\sqrt{3}\lambda_{SO}$ because of the finite-size effect. The crossing edge states inside the gap are the main characteristic of the quantum spin Hall phase.

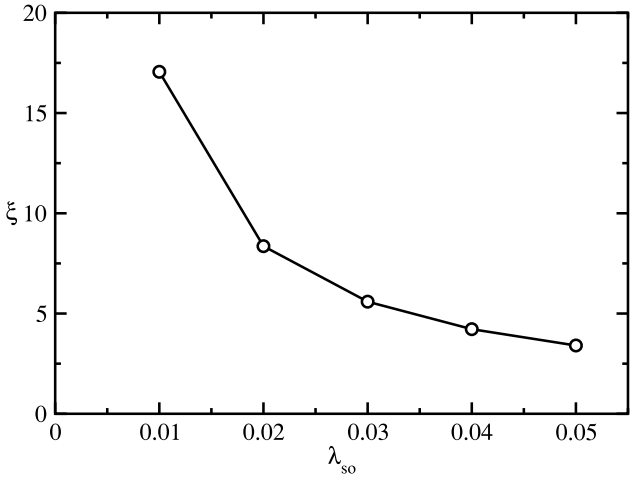

Figure 3. Decay length of the edge state at the Dirac point. The size of the ring is $n_x = 100$ and $n_y = 100$. The decay length is inversely proportional to the strength of the spin–orbit interaction.

value. Therefore, the edge modes for the QSH state should immediately appear, no matter how small the SOI is. In figure 2, we show the energy dispersion for $\lambda_{SO} = 0.01$ and $\Phi = 0$. Overall, the energy spectrum shows intangible changes from the one with $\lambda_{SO} = 0$. However, in the inset one can see that the Dirac point is opened up, with mid-gap edge modes. The edge modes do not merge into bulk bands up to near the boundaries of the Brillouin zone.

The envelope of the probability distribution for the edge state decays exponentially, $|\Psi(x)|^2 \propto \exp(-d/\xi)$, where d is the distance from the edge. As one increases the SOI, the edge states should be more localized. In figure 3, we show the decay length ξ of the edge state at the Dirac point for different values of λ_{SO}. Upon fitting, the inverse of the decay length is about $5.89\lambda_{SO}$, proportional to the SOI. For example, for $\lambda_{SO} = 0.01(0.05)$, the decay length is about 17 sites (three sites). With this result, one can estimate whether, for a given ribbon, the inter-edge coupling could be safely neglected.

At first, we report the PCC *without* SOI. In this case, the current is from bulk states only since there is no edge mode. The PCCs are shown on the left of figure 4. As we mentioned earlier, there is a Dirac point in the energy spectrum when $n_x = 3n + 2$. The discontinuity of the slopes at the Dirac point produces the finite jump at zero flux for $n_x = 50$. On the other hand, systems with $n_x \neq 3n + 2$ are gapped (without the Dirac point), so the PCCs show no jump for $n_x = 51, 52$. Furthermore, the overall magnitude of the PCC is also much smaller.

The plots for the PCCs *with* SOI are shown on the right of figure 4. Even though the SOI introduces little change to the PCC for $n_x = 50$, it has a dramatic effect on the persistent currents of $n_x = 51$ and 52. In the second and third rows of figure 4, the sinusoidal-like variations on the left become sawtooth-like on the right, and have much larger magnitudes (similar to the system with $n_x = 50$). This, of course, is due to the energy level crossing of the newly formed edge modes.

We now focus on the edge *spin* current in the presence of SOI. Spin-resolved edge currents $I_{R\sigma}$ ($I_{L\sigma}$) are shown on the right (left) side of figure 5. The spin-resolved edge current has a discontinuity at $\Phi = 0$, similar to those in figure 4. However, in figure 5, the sawtooth curves ride on background values of ± 1 (i.e. opposite spins move along opposite directions). Therefore, it is a more stable transport with respect to the change of magnetic flux. As n_y gets larger, even though the jump is smaller, the overall magnitudes of these currents remain close to one.

A few symmetries can be observed in figure 5. For example, $I_{L+} = I_{R-}$ and $I_{L-} = I_{R+}$. Also, $I_{R+}(\phi) = -I_{R-}(-\phi)$, similarly for the left edge. Notice that the charge current for the right edge, $I_R = I_{R+} + I_{R-}$, is small but nonzero due to the slight asymmetry between $I_{R\pm}(-\phi)$ and $I_{R\pm}(\phi)$. On the other hand, the spin current for the right edge, $I_R^s = I_{R+} - I_{R-}$, is roughly of value 2 (in units of $t/4\pi$).

In the figure, the persistent spin current is nonzero even if there is no magnetic flux. Such a current, unlike the persistent charge current, does not require the breaking of time-reversal symmetry. However, the edge states being helical is essential. Furthermore, since the magnitude of the edge spin current is not reduced in a larger ring (in contrast to the PCC), it is possible to have it in a large ring (if phase coherence around the ring could be preserved). For a flat sheet with open boundary (and no external bias), the edge spin current cannot persist. A continuous spin circulation without external driving force is possible only in a ring-like structure. In principle, the moving spins would induce an electric dipole [11] (might be oscillating in time) that can be felt. In practice, detecting such an induced electric field remains a great experimental challenge.

3.2. Narrow ribbon

As the ribbon becomes narrower, the edge states on the two sides will couple with each other [26]. Such a coupling may open the Dirac point (when $n_x \neq 3n + 2$) at the Fermi energy.

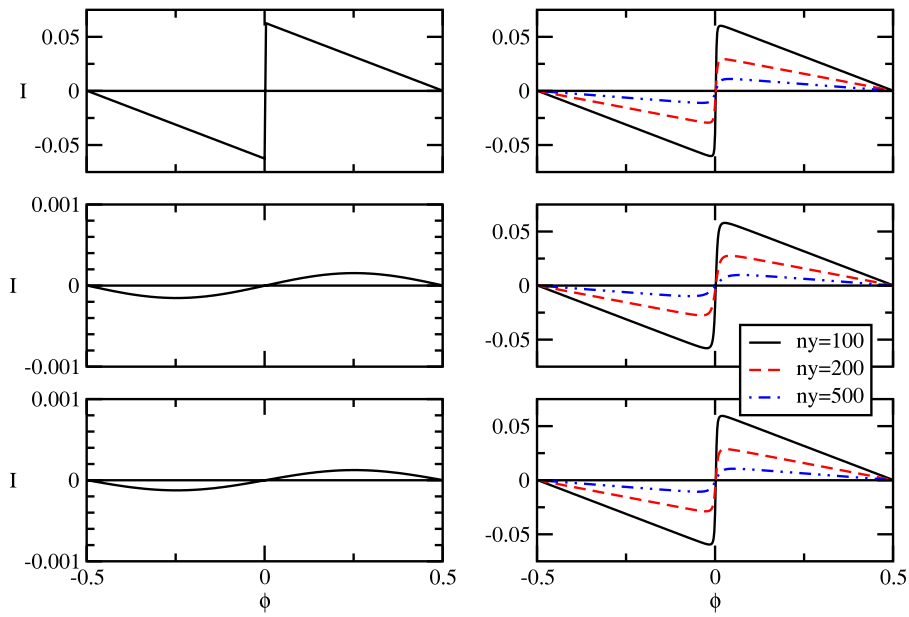

Figure 4. The plots on the left column are the persistent charge currents for $\lambda_{SO} = 0$ and those on the right column are for $\lambda_{SO} = 0.05$. The charge currents are in units of et/h (see equation (7)). The figures on the first, second and third rows are for $n_x = 50$, 51 and 52, respectively. In the right column, one can see that the persistent currents decrease as n_y becomes larger. The magnitudes for the three plots on the right are roughly the same, in sharp contrast to the ones on the left.

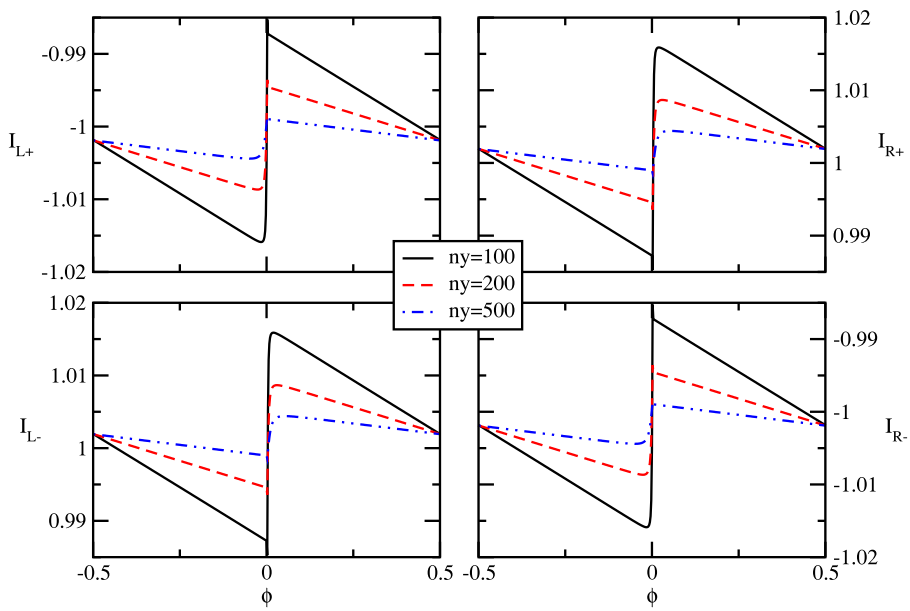

Figure 5. Edge currents for spin-up and spin-down electrons for $n_x = 50$ and $\lambda_{SO} = 0.05$. When n_y is large, the edge persistent current has a smaller discontinuity but the overall magnitude remains close to one.

Figure 6 shows the oscillatory energy gaps for different widths of the ribbon. One can see that the system remains semi-metallic when $n_x = 3n+2$, with or without SOI[7]. When $n_x \neq 3n + 2$, as n_x becomes smaller, inter-edge coupling produces a larger gap (triangles in figure 6). For reference, the bulk gap at $k_y = 0$ is also plotted (solid squares). Notice that the bulk gap is larger at $n_x = 3n+2$, when the energy gap for the edge state vanishes.

For a narrow ribbon, the edge modes are no longer well defined. Therefore, we focus on the total persistent currents carried by the whole ring. Figure 7 shows the persistent currents of spin-up and spin-down electrons in a narrow ring. As one can see, since $I_+ = I_-$, the charge current I is twice the values in figure 7, while the spin current I^s is zero. There could be remnant spin currents along the left and the right edges, but they would cancel each other. For small widths (the left column), the currents for $n_x \neq 3n+2$ can barely be seen[8].

[7] This is true in the tight-binding model, but no longer so in *ab initio* calculations. See [27].

[8] The horizontal lines for $n_x = 15, 16$ do show sinusoidal-like variations after being magnified.

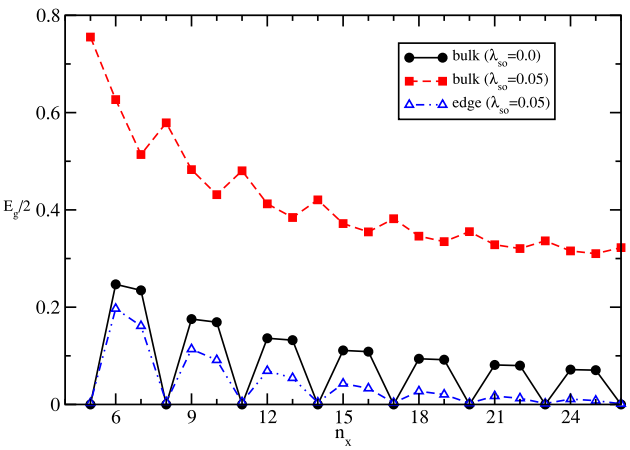

Figure 6. Energy gaps for narrow ribbons with $n_y = 100$. Solid circles are the energy gaps for $\lambda_{SO} = 0$. The system is semi-metallic for $n_x = 3n + 2$, and is insulating otherwise. When $\lambda_{SO} = 0.05$, we show both the edge gaps (triangles) and the bulk gaps (solid squares).

This is due to the finite energy gaps shown in figure 6. The case of $n_x = 3n + 2$ is special since the Dirac point remains closed. Such a dramatic contrast is less apparent in the right column.

3.3. Zeeman interaction

The analysis so far applies to the cases when the electron in the ring feels the Aharonov–Bohm effect through the vector potential of the magnetic flux, but not the magnetic field itself. In the following, we consider a more realistic situation when the graphene ring itself is immersed in a magnetic field. As a result, the electrons can couple with the field through their spins. Some order-of-magnitude estimate is in order: for a ring with n_y sites, the cross-sectional area is $(3/4\pi)n_y^2a^2$ ($a = 2.456$ Å). In order to have one flux quantum inside the ring, the magnetic field needs to be $B \simeq 2.87 \times 10^5/n_y^2$ (in units of T). The Zeeman gap at one flux quantum is $33.25/n_y^2$ eV ($g = 2$). In comparison, the energy difference between neighboring k_y states in the Brillouin zone (see figure 2) is roughly of the order of $2t/n_y$ ($t \simeq 2.8$ eV). Therefore, the Zeeman gap is relatively unimportant, unless n_y is of the order of ten or less.

Figure 8 shows the energy levels near the energy gap (with and without the Zeeman interaction). When $g = 0$, there are two parabolas with a minute energy gap due to the inter-edge coupling. When $g \neq 0$, the upper (and lower) parabola separates into two parabolas. The separation is proportional to the strength of the Zeeman interaction. As a result, it is possible for the upper and lower parabolas to intersect with each other and produce two crossings (two Dirac points). This will alter the qualitative behavior of the $I(\phi)$ curve.

The Zeeman effect on the PCC can be seen in figure 9. Near an integer flux quantum, a vertical jump splits into two (see the inset), due to the two Dirac points in figure 8. Such a split is proportional to the magnitude of the magnetic field. As a result, the $I(\phi)$ curve is no longer periodic in the magnetic flux. This is the main effect of the Zeeman interaction.

3.4. Rashba interaction

For a graphene sheet, the Rashba coupling is possible only if the mirror symmetry with respect to the plane is broken, for

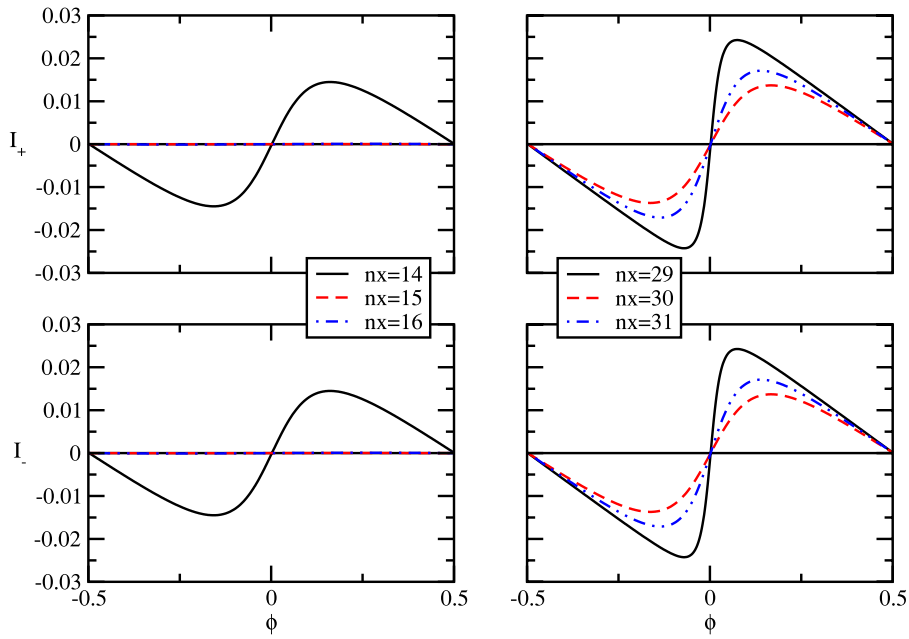

Figure 7. Persistent currents for electrons in a narrow ring with $n_y = 100$ and $\lambda_{SO} = 0.05$. The left column shows the persistent currents for up and down spins when $n_x = 14$–16, while the right column is for $n_x = 29$–31.

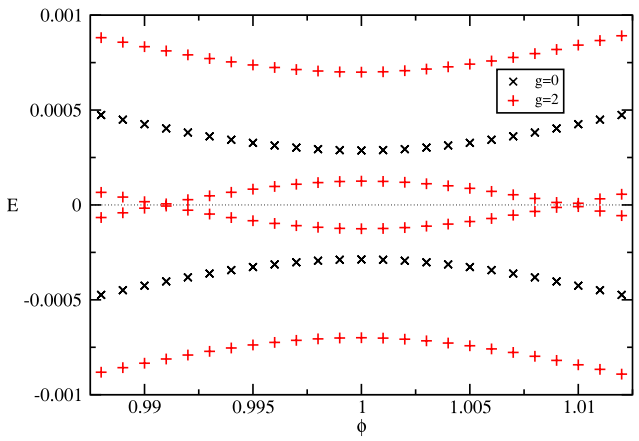

Figure 8. The energy levels near $k_y = 0$ for a ring with $n_x = 50$, $n_y = 100$ and $\lambda_{SO} = 0.01$ are plotted with respect to ϕ near $\phi = 1$. Each curve for $g = 0$ is separated into two curves when g is nonzero.

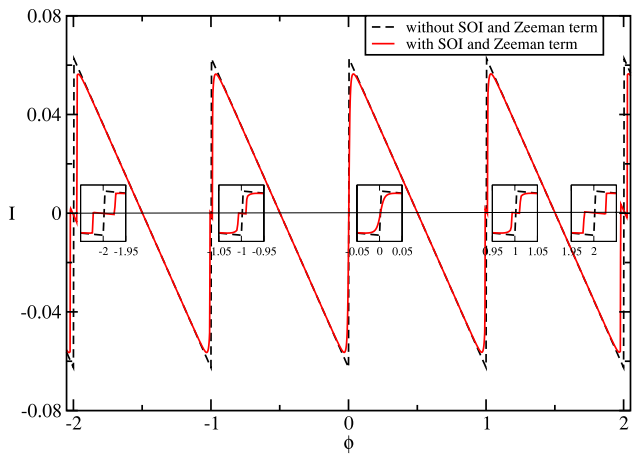

Figure 9. Persistent current for a graphene ring with $n_x = 50$, $n_y = 100$ and $\lambda_{SO} = 0.01$. Insets show magnified views near the jumps.

example, by an electric field or a substrate. For a graphene tube, the Rashba coupling could be induced, for example, by an electric field transverse to the axis of the tube. Kane and Mele found that, if $\lambda_R > 2\sqrt{3}\lambda_{SO}$, then the graphene would no longer be a QSH insulator [2]. For a smaller λ_R, even though the graphene is still in the QSH phase with helical edge states, the electron spins in the edge channels are no longer conserved. Therefore, the magnitude of the edge spin current is reduced. It is interesting to investigate such a reduction in the spin transport. The ring geometry proves to be most convenient since one does not have to worry about the disturbance from external leads.

Figure 10 shows the magnitude of the edge spin currents. When $\lambda_R = 0$, the magnitude is very close to 2. It gradually decreases to zero at the critical value of $\lambda_R = 2\sqrt{3}\lambda_{SO}$, beyond which the graphene is semi-metallic [2] and there is no more edge spin current. Overall, the spin currents for spin-x and spin-y (calculated from semiclassical expressions similar to equation (8)) remain small for the whole range of the Rashba coupling. One can see that,

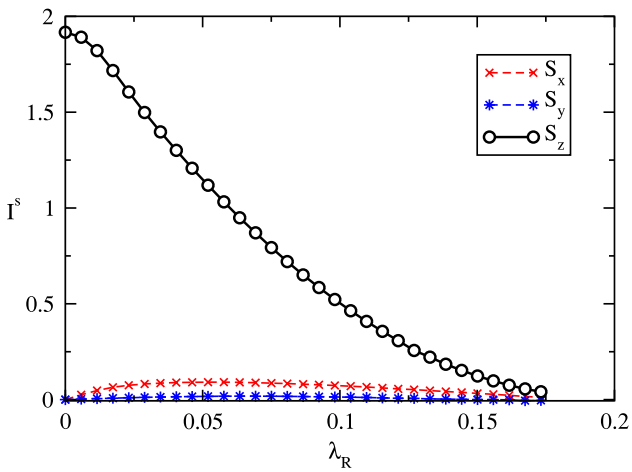

Figure 10. Reduction of the edge spin currents (in units of $t/4\pi$) due to the Rashba coupling. The parameters are $n_x = 50$, $n_y = 100$ and $\lambda_{SO} = 0.05$, and the Zeeman coupling is not considered.

even if λ_R is as large as λ_{SO}, the spin current is still dominated by the spin-z component. The slight deviation from the ideal values of 2 and 0 on both ends is a result of the finite-size effect and inter-edge coupling. Similar reduction of the spin in edge states, when the spin is not conserved, has been observed in various spin-resolved measurements of angle-resolved photo-emission spectroscopy on three-dimensional topological insulators [28].

4. Conclusion

By adding a spin–orbit interaction to a graphene ribbon, one can generate helical edge states along armchair edges. When the ribbon is wrapped to form a ring that encloses a magnetic flux, there are persistent charge and spin currents. We studied the persistent currents in rings with different radii and widths. The bulk state contribution to the currents vanishes if the radius of the ring is large, but the edge state contribution persists. For broad ribbons, the decay length of the edge mode at the Dirac point is inversely proportional to λ_{SO}. The persistent spin current for one helical edge is roughly $t/2\pi$. For narrow ribbons, inter-edge coupling between the edge states opens the Dirac point (when $n_x \neq 3n + 2$) and reduces the persistent currents. For most of the parameters being studied, the Zeeman effect is too small to have much influence. On the other hand, the Rashba coupling is found to deteriorate the edge spin transport, which vanishes beyond a critical value when the graphene is no longer a QSH insulator. Our work shows that the tubular QSH insulator driven by a magnetic flux is an ideal configuration for theoretically exploring the edge transport.

Finally, a remark on the effect of electron–electron interaction, which is beyond the scope of this work. In [23], it has been shown that the Hubbard-type short-ranged interaction could induce edge magnetization. This is related to the following fact: the honeycomb lattice is bipartite and the Hubbard interaction tends to induce antiferromagnetic order. For a zigzag edge, since the lattice points along the

edge are from the same sub-lattice, their spins would point to the same direction. That is the main reason why a zigzag edge is ferromagnetic. This mechanism will not work well for the armchair edge as it contains lattice points from both sub-lattices. Therefore, magnetization induced by the Hubbard interaction is less likely for the armchair edge.

Acknowledgment

The authors would like to acknowledge the financial support from the National Science Council of Taiwan.

References

[1] Hasan M Z and Kane C L 2010 *Rev. Mod. Phys.* **82** 3045
[2] Kane C L and Mele E J 2005 *Phys. Rev. Lett.* **95** 146802
Kane C L and Mele E J 2005 *Phys. Rev. Lett.* **95** 226801
[3] Min H, Hill J E, Sinitsyn N A, Sahu B R, Kleinman L and MacDonald A H 2006 *Phys. Rev.* B **74** 165310
[4] Weeks C, Hu J, Alicea J, Franz M and Wu R 2011 *Phys. Rev.* X **1** 021001
[5] Nakada K, Fujita M, Dresselhaus G and Dresselhaus M S 1996 *Phys. Rev.* B **54** 17954
[6] Buttiker M, Imry Y and Landauer R 1983 *Phys. Lett.* A **96** 365
Cheung H F, Gefen Y, Riedel E K and Shih W H 1988 *Phys. Rev.* B **37** 6050
Cheung H F, Gefen Y and Riedel E K 1988 *IBM J. Res. Dev.* **32** 359
[7] Levy L P, Dolan G, Dunsmuir J and Bouchiat H 1990 *Phys. Rev. Lett.* **64** 2074
Chandrasekhar V, Webb R A, Brady M J, Ketchen M B, Gallagher W J and Kleinsasser A 1991 *Phys. Rev. Lett.* **67** 3578
[8] Bleszynski-Jayich A C, Shanks W E, Peaudecerf B, Ginossar E, von Oppen F, Glazman L and Harris J G E 2009 *Science* **326** 272
[9] Loss D, Goldbart P and Balatsky A V 1990 *Phys. Rev. Lett.* **65** 1655
Loss D and Goldbart P M 1992 *Phys. Rev.* B **45** 13544
[10] Splettstoesser J, Governale M and Zülicke U 2003 *Phys. Rev.* B **68** 165341
[11] Schütz F, Kollar M and Kopietz P 2003 *Phys. Rev. Lett.* **91** 017205
[12] Schütz F, Kollar M and Kopietz P 2004 *Phys. Rev.* B **69** 035313
Wu J N, Chang M C and Yang M F 2005 *Phys. Rev.* B **72** 172405
[13] Lin M F and Chuu D S 1998 *Phys. Rev.* B **57** 6731
[14] Recher P, Trauzettel B, Rycerz A, Blanter Y M, Beenakker C W J and Morpurgo A F 2007 *Phys. Rev.* B **76** 235404
[15] Schelter J, Bohr D and Trauzettel B 2010 *Phys. Rev.* B **81** 195441
[16] Ma M M and Ding I W 2010 *Solid State Commun.* **150** 1196–9
[17] Dutta P, Maiti S K and Karmakar S N 2011 arXiv:1105.3036
[18] Peng H, Lai K, Kong D, Meister S, Chen Y, Qi X L, Zhang S C, Shen Z X and Cui Y 2010 *Nature Mater.* **9** 225
[19] Bardarson J H, Brouwer P W and Moore J E 2010 *Phys. Rev. Lett.* **105** 156803
[20] Zhang Y and Vishwanath A 2010 *Phys. Rev. Lett.* **105** 206601
[21] Michetti P and Recher P 2011 *Phys. Rev.* B **83** 125420
[22] Chang K and Lou W K 2011 *Phys. Rev. Lett.* **106** 206802
[23] Soriano D and Fernández-Rossier J 2010 *Phys. Rev.* B **82** 161302
[24] Huertas-Hernando D, Guinea F and Brataas A 2006 *Phys. Rev.* B **74** 155426
[25] Wu S T and Mou C Y 2003 *Phys. Rev.* B **67** 024503
Also, see Wu S T and Mou C Y 2002 *Phys. Rev.* B **66** 012512
Huang B L, Wu S T and Mou C Y 2004 *Phys. Rev.* B **70** 205408
[26] Shan W Y, Lu H Z and Shen S Q 2010 *New J. Phys.* **12** 043048
[27] Son Y W, Cohen M L and Louie S G 2006 *Phys. Rev. Lett.* **97** 216803
[28] See, for example Hsieh D *et al* 2009 *Nature* **460** 1101